Weierstraß-Institut
für Angewandte Analysis und Stochastik

im Forschungsverbund Berlin e.V.

Preprint ISSN 0946 – 8633

Semiconductor laser under resonant feedback from a Fabry-Perot: Stability of continuous wave operation

Vasile Z. Tronciu[1], Hans-Jürgen Wünsche[2], Mindaugas Radziunas[3],

Matthias Wolfrum[3]

submitted: 9th September 2005

[1] Department of Physics
Technical University of Moldova
Stefan cel Mare av. 168
Chisinau MD-2004
Republic of Moldova
E-Mail: tronciu@mail.utm.md

[2] Institute of Physics
Humboldt University Berlin
Newtonstr. 15
12489 Berlin
Germany
E-Mail: ede@physik.hu-berlin.de

[3] Weierstrass Institute for Applied
Analysis and Stochastics
Mohrenstr. 39
10117 Berlin
Germany
E-Mail: radziuna@wias-berlin.de
E-Mail: wolfrum@wias-berlin.de

No. 1051

Berlin 2005

Key words and phrases. semiconductor laser, delayed feedback control, stability analysis.

1999 *Physics and Astronomy classification Scheme.* 42.65.Sf, 42.55.Px, 42.60.Da, 02.30.Lt.

Edited by
Weierstraß-Institut für Angewandte Analysis und Stochastik (WIAS)
Mohrenstraße 39
10117 Berlin
Germany

Fax: + 49 30 2044975
E-Mail: preprint@wias-berlin.de
World Wide Web: http://www.wias-berlin.de/

Abstract

We study the continuous-wave (CW) operation of a semiconductor laser subject to optical feedback from a Fabry-Perot resonator in a case where the emission is resonant to a reflection minimum of the resonator. This configuration is treated in the framework of Lang-Kobayashi equations. The nature of bifurcations and the stability of steady state solutions is analyzed in dependence on magnitude and phase of the feedback. In contrast to conventional optical feedback from a single mirror, the locus of external cavity modes is no more elliptic but represents a tilted eight with possible satellite bubbles. Below a critical feedback strength, which is analytically given, only one single mode exists representing the completely unchanged CW emission of the laser. In this weak-feedback regime, the feedback phase allows a noninvasive control of the CW emission and a tailoring of its small-signal response within wide limits. The obtained results are prototype for all-optical realizations of delayed feedback control.

1 Introduction

Stabilization of laser emission by external cavities is long established [2, 3, 4, 1] and of continuous interest [5, 6]. Fabry-Perot (FP) cavities are mostly operated as optical filters, which suppress all waves which do not fit to the narrow spectral resonances [3, 4, 5]. Only exception, to our knowledge, is the powerful Pound-Drever-Hall technique [2], which exploits a resonant minimum of the FP reflectivity in order to derive an electronic control signal used to lock the laser cavity to the FP resonance.

In difference to all these methods, we consider stability control by direct optical feedback from an FP with mirror-reflectivity R and round trip time τ_{FP} (Fig. 1). Under ideal conditions, in particular no loss and equal phase and group velocities, the feedback field is

$$\mathcal{E}_{\mathrm{b}}(t) = K \sum_{n=0}^{\infty} R^n \cdot [\mathcal{E}(t_n) - \mathcal{E}(t_n - \tau_{\mathrm{FP}})]. \tag{1}$$

$\mathcal{E}(t)$ represents the field amplitude emitted by the laser. $t_n = t - \tau_l - n\tau_{\mathrm{FP}}$ is delayed by n round trips in the resonator plus the round trip time τ_l between laser and resonator. K measures the magnitude of feedback, including a possible attenuation between FP and laser.

We focus to a case, where the laser without feedback is assumed to emit continuous wave (CW) with a single frequency ω_0 resonant to the FP, i.e., $\omega_0\tau_{\mathrm{FP}}$ is an integer multiple of 2π. In this particular case, $\mathcal{E}$ is τ_{FP}-periodic and the feedback field $\mathcal{E}_{\mathrm{b}}$ becomes zero. Thus, the free running state of the laser is not modified by the presence of the resonant FP. One might wonder whether the resonator has any influence at all. However, perturbations and noise cause deviations from the ideal state giving rise to a nonzero feedback, which in turn modifies the response of the laser to the perturbations. Thus, the considered feedback configuration does not change the laser state itself but its stability properties.

Delayed feedback of type (1), originally introduced by Pyragas and Socolar [7, 8, 9], is well known as a general and self-adaptive method for noninvasive control of dynamical systems. It has been widely used to stabilize unstable periodic orbits within chaos [7, 8, 9, 10] and

it is also able to improve the coherence of oscillatory motion under the impact of noise [11, 12]. Already one decade ago, Socolar et al. [8, 9] noticed that feedback from a FP should allow an all-optical implementation of this general control scheme. Surprisingly, no in-depth study of such an implementation exists until now, although first numerical explorations [13, 14, 15] of similar interferrometric configurations gave examples for the possibility of an all-optical chaos control. The lack of progress is supposably related to the multiple time scales being specific for all-optical configurations [13]. They range over more than six orders of magnitude from the femtoseconds of the optical oscillations over hundreds of picoseconds for inversion oscillations up to round-trip cycles of several nanoseconds in the long-cavity configurations considered in Refs. [13, 14, 15]. In difference to other applications of the Pyragas-Socolar schema, oscillations on the longer time scales are to be controled here with an interferrometric feedback that is sensitive to the shorter time scales, too. Indeed, using the standard scaling $\mathcal{E}(t) = \mathrm{Re}\{E(t)\exp i\omega_0 t\}$ onto slowly varying amplitudes $E(t)$, Eq. (1) transforms to

$$E_\mathrm{b}(t) = \mathcal{K}\sum_{n=0}^{\infty}\mathcal{R}^n[E(t_n) - e^{-i\phi}E(t_n - \tau_\mathrm{FP})], \tag{2}$$

with $\mathcal{K} = Ke^{-i\varphi}$ and $\mathcal{R} = Re^{-i\phi}$. It differs from the conventional Pyragas-Socolar feedback by being complex valued and by the presence of the two optical phase shifts $\varphi = \omega_0\tau_l$ and $\phi = \omega_0\tau_\mathrm{FP}$ If phase and group velocities differ from each other, $\varphi = 2l\omega_0/c_p$ and $\phi_\mathrm{FP} = 2L\omega_0/c_p$ are governed by the phase velocity c_p, in contrast to the round-trip times $\tau_l = 2l/c_g$ and $\tau_\mathrm{FP} = 2L/c_g$, which are determined by the group velocity c_g. Incorporation of possible phase shifts by the mirrors is also straightforward. Obviously, the impact of this control term depends sensitively on both phases. This very fact opens new degrees of freedom for tailoring the feedback control but it also requires to master the geometry of the configuration on length scales small compared to the wavelength. Fortunately, continuing technological progress of multi-section lasers (see, e.g., Ref. [16]) brings into reach correspondingly stable configurations (Fig. 1) with integrated common waveguides and with phase shifts tunable by injection currents.

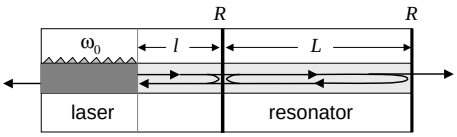

Figure 1: Schematic view of a single-mode DFB laser coupled to a Fabry-Perot resonator. R: mirror reflectivity, L: resonator length, l: distance between laser and resonator. By the finite group velocity c_g, the geometry causes two time delays, the round trip times $\tau_\mathrm{FP} = 2L/c_g$ and $\tau_l = 2l/c_g$ within the FP and between laser and FP, respectively.

The present paper represents a first theoretical study of such a configuration. In view of the complexity of the problem, we restrict the analysis to a special case under some simplifying assumptions. Stable single-mode emission of the solitary laser is assumed, being resonant to the FP, i.e., $\phi \bmod 2\pi = 0$. Having integrated devices in mind, a short FP cavity is considered with small reflectivity R, allowing to neglect multiple reflections. The analysis bases on the well-known Lang-Kobayashi equations [17], generalized to feedback of type (2), which are introduced in Section 2. Analytic equations are derived in Section 3 for the external cavity modes (ECM) and evaluated for an example set of parameters. In Section 4, we focus on the bifurcations introduced by the resonant feedback from the FP and on its impact on the local and global stability of laser states. Feedback strength

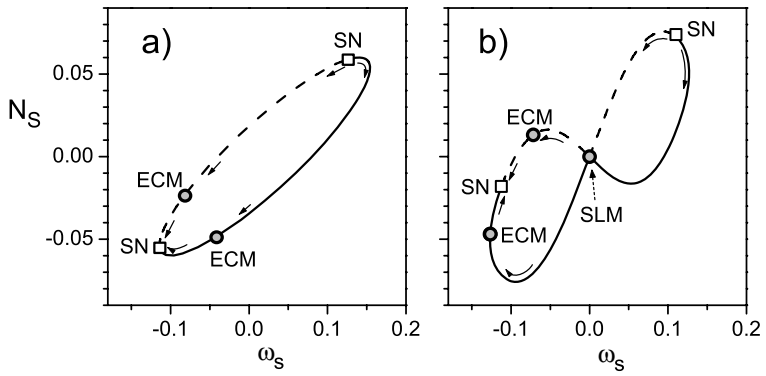

Figure 2: Curves of ECMs in the (ω, N) plane for $K = 0.05$. a) conventional optical feedback. b) resonant feedback from Fabry-Perot cavity. SN: saddle-node bifurcation. ECM: external cavity mode at a particular feedback phase. SLM: solitary laser mode. Solid line: node. Dashed: saddle. Arrows indicate how the ECM move with increasing feedback phase. SLM keeps in its position independent of phase.

K and phase φ are considered as main bifurcation parameters. The particular impact of the Fabry-Perot on frequency and damping of relaxation oscillation is evaluated in Section 5. Finally, conclusions are drawn in section 6.

2 Model and equations

In this section we will discuss the laser setup and a model for a single mode DFB laser under the influence of an resonant feedback from a Fabry-Perot resonator (RFFP). Such a configuration is shown schematically in Fig. 1. We will use a Lang-Kobayashi type system [17] for the complex field amplitude E and an excess carrier density N. In dimensionless form, it is given by [18]

$$\frac{dE}{dt} = (1 + i\alpha)NE + E_{\mathrm{b}}(t), \tag{3}$$

$$\frac{dN}{dt} = \frac{1}{T}(J - N - (2N + 1)\,|E|^2) \tag{4}$$

where J is an excess pump current, T is the ratio of the carrier lifetime and the photon lifetime, and α is the linewidth enhancement factor. The time is measured in units of photon lifetime. As mentioned above, we focus to the resonant case $\phi = 0$, i.e., the CW emission of the unperturbed laser is at a minimum of the FP reflectivity. Additionally we assume a small reflectivity $R \ll 1$ and account only for one round trip in the air gap and in the Fabry-Perot cavity. In this case the feedback term can be written as

$$E_{\mathrm{b}}(t) = Ke^{-i\varphi}\left[E(t - \tau_l) - E(t - \tau)\right], \tag{5}$$

where $\tau = \tau_l + \tau_{\mathrm{FP}}$. Note that K is also rescaled by choosing the nondimensional LK model.

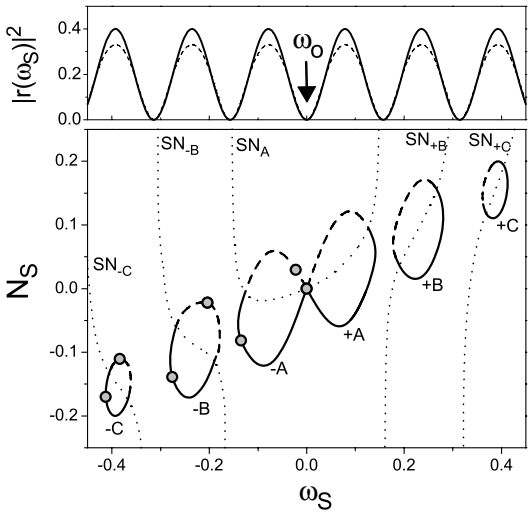

Figure 3: Top panel: reflection spectrum of a Fabry Perot resonator with mirror reflectivity $R = 0.1$. Solid line: $n = 0$ contribution of Eq. (2). Dashed: including all multiple round-trips in the resonator. Arrow: resonant position of the solitary laser frequency ω_0. Lower panel: Location of ECMs of system (3)-(5) for $K = 0.1$. Circles: ECMS for fixed $\varphi = 0$. Dotted: saddle-node curves (SN) separating between modes and antimodes.

3 External cavity modes (ECM)

We begin our analysis by studying stationary lasing states of system (3)-(5). They are given by rotating wave solutions of the form

$$E(t) = E_S e^{i\omega_S t}, N = N_S, \tag{6}$$

which are usually called the external cavity modes (ECMs). Inserting (6) into (3) and splitting the equation into real and imaginary parts, we obtain

$$N_S = K\left[-\cos(\varphi + \omega_S\tau_l) + \cos(\varphi + \omega_S\tau)\right] \tag{7}$$

$$\omega_S - \alpha N_S = K\left[-\sin(\varphi + \omega_S\tau_l) + \sin(\varphi + \omega_S\tau)\right]. \tag{8}$$

The carrier equation (4) can be used to obtain the output intensity

$$|E_S|^2 = \frac{J - N_S}{2N_S + 1} \tag{9}$$

Finally, inserting (7) into (8), we obtain

$$\begin{aligned} \omega_S &= \alpha K[\cos(\varphi + \omega_S\tau) - \cos(\varphi + \omega_S\tau_l)] \\ &+ K[\sin(\varphi + \omega_S\tau) - \sin(\varphi + \omega_S\tau_l)]. \end{aligned} \tag{10}$$

Note that the equations for ECMs of a laser with simple optical feedback (see e.g. [19]) can be obtained from (7)-(10) by just dropping all terms containing τ_l. In this case it is well known that in the (ω, N)-plane, the ECMs are located on ellipses. For feedback

$$K < \frac{1}{\tau\sqrt{1+\alpha^2}},$$

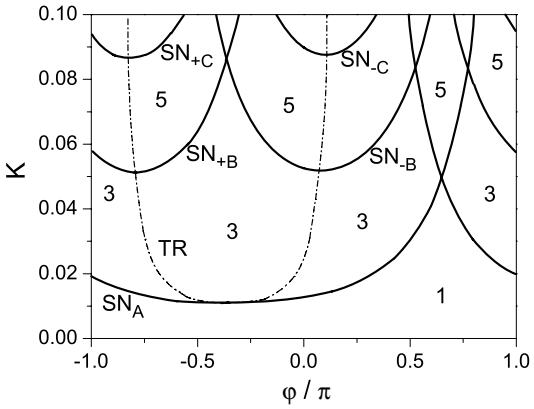

Figure 4: Lines of saddle-node (SN) and transcritial (TR) bifurcations at different locations; number of ECMs in corresponding regions

there is only one ECM, moving along the ellipse for varying phase φ. For feedback strength K above this critical value, larger numbers of ECMs appear with increasing K. Varying φ, they appear and disappear in pairs at saddle-node bifurcations at the top and the bottom end of the ellipse (see Fig. 2a, or [19] for more details). In contrast to this situation, we have for RFFP always an ECM in the origin, which we denote as solitary laser mode. This is due to the fact that at resonance the CW emission of the laser does not get any feedback. However, as we will see later, its stability properties will change drastically. Below the critical feedback level

$$K_c = \frac{1}{\tau_{\mathrm{FP}}\sqrt{1+\alpha^2}}, \tag{11}$$

there can exist only the solitary laser mode. For larger feedback, additional ECMs can appear again in pairs at saddle-node bifurcations. For varying phase φ they move now along a figure eight, meeting the solitary laser mode, which is sitting in the waist, at transcritical bifurcations (see Fig. 2b). For larger values of K, additional to the figure eight there appear satellite bubbles of ECM locations, located around neighbouring reflectivity maxima of the FP resonator, see Fig. 3. Differentiating (10), we obtain the condition for saddle-node bifurcations:

$$\begin{aligned} 1 = \quad & K[\alpha\tau_l \sin(\varphi+\omega_S\tau_l) - \alpha\tau\sin(\varphi+\omega_S\tau) \\ & - \tau_l\cos(\varphi+\omega_S\tau_l) + \tau\cos(\varphi+\omega_S\tau)] \end{aligned} \tag{12}$$

This equation together with the ECM conditions (7) and (8) can now be solved numerically. We fixed the parameters

$$\alpha = 2, J = 0.3, T = 1000, \tau_l = 0.001, \tau_{\mathrm{FP}} = 40, \tag{13}$$

and varied feedback strengt K and phase φ. In the lower part of Fig. 3, we show the situation in the (ω, N)-plane: the saddle-node curves separate the ECMs on the figure eight and their satellites in saddles and nodes. They are usually called antimodes and modes, respectively. The antimodes (dashed) are always unstable, the modes (solid) are stable until they destabilize in a Hopf bifurcation, which we discuss in the next section. Figure

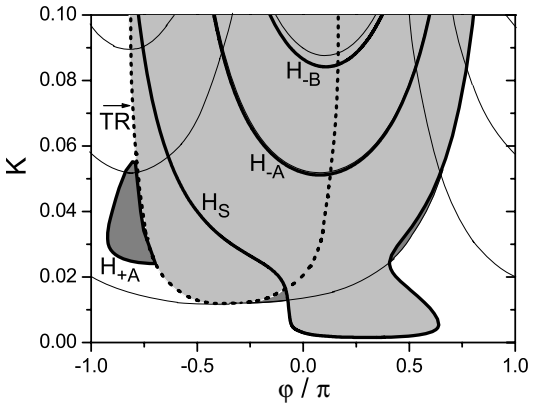

Figure 5: Hopf bifurcations of stable ECMs at different locations (thick solid): Solitary laser mode (H_S), ECMs on the right (H_{+A}) and left (H_{-A}) part of the figure eight, and on satellites (H_{+B}, H_{-B}). Stability of the central mode. White area: CW operation. Light-grey region: unstable regime of central mode. Dark-grey regions: bistability between central and first modes. Thick dotted line: transcritical bifurcation. Thin solid line: saddle-node bifurcation.

4 shows the corresponding bifurcation scenario in the plane of the feedback parameters K and φ. Additional ECMs appear on the figure eight at the curve of saddle-node bifurcations SN_A. On the satellites $(+B, -B, +C, -C, \dots)$, the corresponding bifurcation curves are $SN_{+B}, SN_{-B}, SN_{+C}, SN_{-C}, \dots$. At the transcritical bifurcation line TR, ECMs move from the left part $+A$ of the figure eight to the right part $-A$. Note that the degenerate point, where the transcritical bifurcation meets the saddle-node, represents a codimension 3 bifurcation, which is not completely unfolded here since we have fixed the resonance condition.

4 Stability of ECMs

In the following we use the software DDE-BIFTOOL [20] to study the stability properties of the ECM solutions discussed above. To this end, it is necessary to use the ECM frequency as reference frequency, which transforms the rotating wave into a stationary solution. In this way, ω_S is considered as an extra free parameter. To exclude the degeneracy originating from the phase shift invariance, one has to induce an additional constraint, e.g. $\mathrm{Re}(E_S) = 0$.

It turns out that there are three different possibilities for Hopf bifurcations of stable ECMs (see Fig.5).

- The solitary laser mode in the waist of the figure eight can become unstable in a Hopf bifurcation (H_S). This can happen even for feedback $K < K_c$, where the solitary laser mode is the only existing ECM.
- On the left part $-A$ of the figure eight and on the left satellites $(-B, -C, \dots)$, stable ECMs originate from the saddle-node bifurcation. They can become unstable for further increasing φ at the corresponding Hopf curves $H_{-A}, H_{-B}, \dots$. This happens only for a sufficiently large feedback level K.

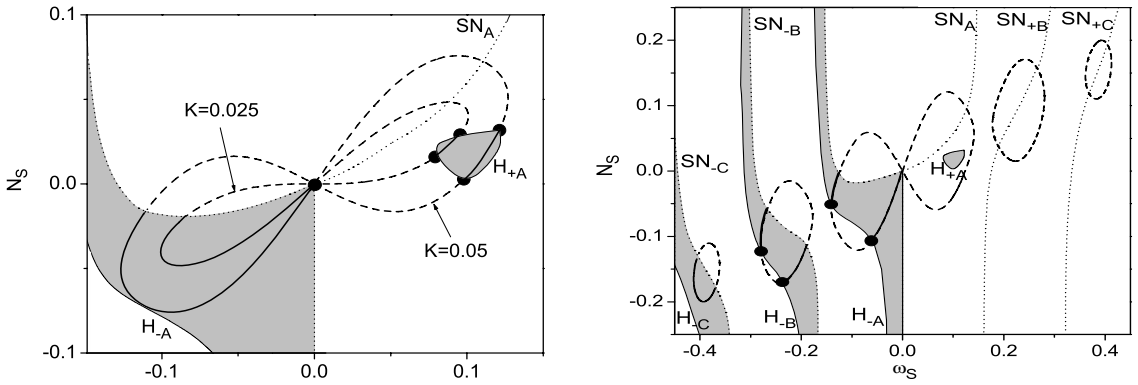

Figure 6: Region of stable ECMs in the (N_S, ω_S)-plane (shaded), bounded by lines of Hopf bifurcations (thin solid) and saddle-node bifurcations (dotted). Left panel: with figure eight for $K = 0.025$ and $K = 0.05$. Right panel: with figure eight and satellite bubles for $K = 0.1$. Thick solid: location of stable ECMs. Thick dashed: location of unstable ECMs. Full circles: Hopf bifurcation points for fixed values of K. Labels as in Fig. 3.

- On the right part $+A$ of the figure eight and on the right satellites $(+B, +C, \dots)$, all ECMs are unstable, in general. Only in a small island on $+A$, bounded by the Hopf curve H_{+A}, they are stable.

The location of stable ECMs in the (ω, N)-plane is given by the shaded region in Fig. 6. Note that the vertical line at $\omega_S = 0, N < 0$ is not a bifurcation curve, because, as at the other reflectivity minima of the resonator, ECMs do not exist there. Only in the limit of infinite K, ECMs do approach this line.

Figure 7 shows a specific bifucation scenario for fixed $K = 0.05$. Figure 8 resembles the situations φ fixed to 0 and -0.65π. Note that for $\varphi = 0$, the solitary laser mode destabilizes already for very small values of K. Collecting all bifurcations of the solitary laser mode, we can determine its stability region. In Fig. 5, the region of instability of the solitary laser mode is shaded in light grey. In dark grey, we indicated regions of coexistence with another stable ECM (bistability). For large feedback, there might exist other stable objects (e.g. periodic solutions) which we have not captured in our calculations.

As one expects from optical feedback, the feedback phase has a decisive role, whether the feedback acts stabilizing or destabilizing to the solitary laser mode. In the next section we perform a detailed study on the linear stability properties of the solitary laser mode.

5 Relaxation oscillations

Now we consider the control of relaxation oscillations by the resonator. To this purpose, the system (3)-(5) is linearised in the form

$$\frac{d}{dt}\vec{\nu}(t) = A\vec{\nu}(t) + B\vec{\nu}(t-\tau_l) + C\vec{\nu}(t-\tau) \tag{14}$$

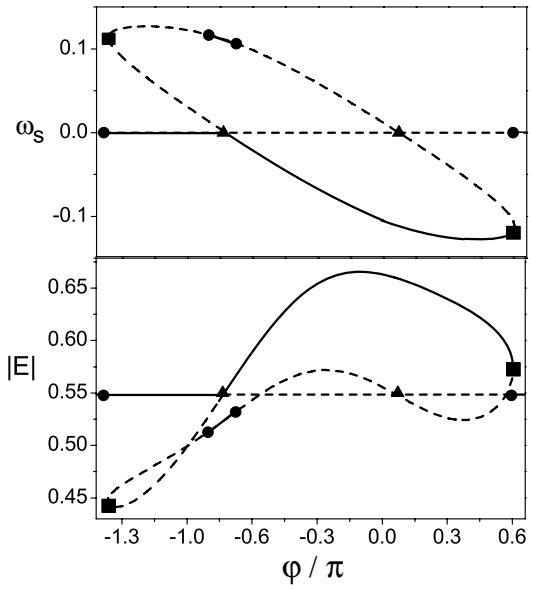

Figure 7: Bifurcation diagrams for $K = 0.05$. Upper panel: (ω_S, φ) plane. Lower panel: $(|E|, \varphi)$ plane. Transcritical and Hopf bifurcations are marked by triangles and circles, respectively. Solid lines: stable stationary solutions; dashed lines: unstable ones. Squares: saddle-node bifurcations.

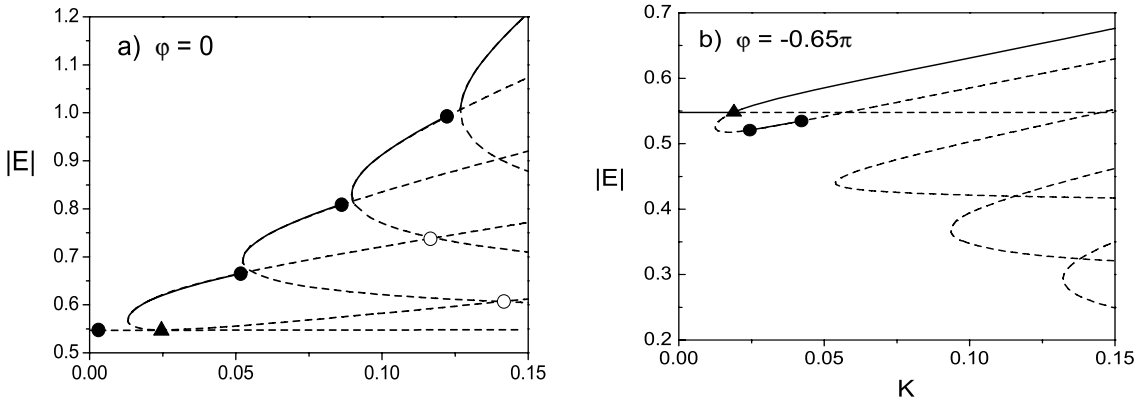

Figure 8: Bifurcation diagram of the steady states in the plane $|E|$ vs the feedback strength K for $\varphi = 0$ and $\varphi = -0.65\pi$. The solid lines show the stable stationary solutions. Circles indicate the Hopf bifurcation points. The empty circles denote the Hopf-bifurcation which appears on unstable branches. The triangle denotes transcritical bifurcation.

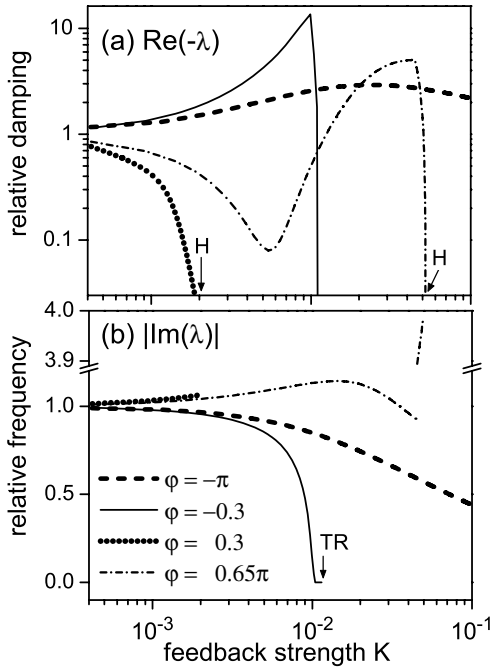

Figure 9: Solutions λ of the characteristic equation (15) for the central mode versus feedback strength K. Only the respective solution with lowest $\mathrm{Re}\lambda < 0$ is shown. (a) $\gamma = -\mathrm{Re}\lambda$ and (b) $\omega = |\mathrm{Im}\lambda|$ correspond to damping and frequency of relaxation oscillations, respectively. H and TR label Hopf and transcritical bifurcations, respectively. The curves are normalized to the values without feedback. Parameters: Eq. (13).

where $\vec{v}(t) = (\mathrm{Re}E(t) - E_1, \mathrm{Im}E(t) - E_2, N(t) - N_S)$ represents the deviation from field $E_S = E_1 + iE_2$ and carrier density N_S of a selected ECM. The matrics A, B and C are

$$
\begin{aligned}
A &= \begin{pmatrix} N_S & \omega_S - \alpha N_S & E_1 - \alpha E_2 \\ \alpha N_S - \omega_S & N_S & E_2 + \alpha E_1 \\ -2E_1 G/T & -2E_2 G/T & -(1+2|E_S|^2)/T \end{pmatrix} \\
B &= K \begin{pmatrix} \cos(\varphi) & \sin(\varphi) & 0 \\ -\sin(\varphi) & \cos(\varphi) & 0 \\ 0 & 0 & 0 \end{pmatrix} \\
C &= -K \begin{pmatrix} \cos(\psi) & \sin(\psi) & 0 \\ -\sin(\psi) & \cos(\psi) & 0 \\ 0 & 0 & 0 \end{pmatrix}
\end{aligned}
$$

with $G = 1 + 2N_S$, $\varphi = \varphi + \omega_S \tau_l$, and $\psi = \varphi + \omega_S \tau$. The characteristic equation for eigenvalues of this linear system has the form

$$\chi(\lambda) = \det(\lambda E - A - e^{-\lambda \tau_l} B - e^{-\lambda \tau} C) = 0, \tag{15}$$

which determines the complex parameter λ. The real and imaginary parts of $-\lambda$ correspond in general to decay rates γ and oscillation frequencies ω, respectively, of small deviations from the ECM.

In the special case of a solitary laser, one has $K = 0, N_S = 0, \omega_S = 0$ and $|E_S|^2 = J$ and one gets the known expressions for damping and frequency of relation oscillations (RO),

which are $\gamma = (1+2J)/2T$ and $\omega = \sqrt{J/T}$, respectively, in lowest order of $1/T$. These quantities determine important parameters of lasers like small signal response, relative intensity noise (RIN), and chirp (see, e.g., chapter 6 of Ref. [21]).

To highlight control of these properties by the resonator, we have calculated the nonzero roots of Eq. (15) for the central mode in dependence on feedback strength K and phase φ. Plots of λ versus K are shown in Fig. 9 for some particular phases φ representing the different regions in Fig. 5. Note that $\varphi = \pm\pi$ corresponds to the standard Pyragas-type of delayed feedback control. Accordingly, the solitary laser mode keeps always stable with slightly enhanced damping and reduced frequency of relaxation oscillations (thick dashed in Fig. 9). At $\varphi = 0.3\pi$ (thick dotted), the RO-damping drops rapidly down towards the Hopf bifurcation H at $K \approx 0.002$. The frequency variation is negligible in this tiny interval. A transition from weak damping to overdamping manifests in case $\varphi = -0.3$ (solid). The decay rate first increases with K, passes a kink, and falls dramatically towards the transcritical bifurcation TR. At the kink, the frequency gets zero and the damping enhanced by more than one order of magnitude. Perturbations decay rapidly (within few ten ps) and monotoneously in this regime. Such behaviour is possibly of high interest for high-speed modulation of the laser. A similar high damping with a kink and subsequent sudden decrease appears also for $\varphi = 0.65\pi$ (dash-dotted) just before the Hopf bifurcation H. As before, this scenario is related to the proximity of a saddle-node bifurcation of two other ECM (cf. Fig. 5). However, the frequency keeps finite here and it even jumps to much higher values beyond the kink. The dip in the damping around $K \approx 0.005$ is caused by the influence of the nearby Hopf bifurcation curve H_S, see Fig. 5. Altogether, these examples demonstrate interesting possibilities to control the small-signal dynamics of a laser without changing its CW output.

6 Conclusion

In the framework of properly adapted Lang-Kobayashi equations, we have treated a single-mode semiconductor laser under resonant optical feedback from a Fabry-Perot cavity. Evaluation of mode spectra and of the most relevant bifurcations in dependence of magnitude and phase of the feedback leads to a comprehensive picture. Below a critical feedback strength K_c, analytically given in Eq. (11), only one single mode exists. It represents the completely unchanged CW emission of the laser. Although the solitary laser mode keeps unmodified by the resonator, the stability of it changes drastically. The effects range from destabilization of relaxation oscillations in Hopf bifurcations to transitions into overdamped behaviour, in sensitive dependence on the feedback phase. Thus, this weak-feedback regime allows a wide control of the small-signal performance of the laser without feedback-induced changes of the laser state. If the feedback increases beyond K_c, an increasing number of additional external cavity modes (ECM) appear as mode-antimode pairs in saddle-node bifurcations. Transcritical bifurcations as well as multistability reduce the local and global stability of the solitary laser mode in this regime.

The obtained results are prototype for all-optical realizations of delayed feedback control (DFC). The optical phase generally appears as a new control parameter, which is not present in standard DFC. Maximum stability against perturbations has been obtained at a feedback phase different from π that corresponds to standard DFC. The round-trip phase shift in the FP must equal an integer multiple of 2π in order to get noninvasive

control. For an attempted noninvasive stabilization of periodic intensity-pulsations, the group round-trip time will have to match the pulsation period in addition. Our result on the critical feedback strength K_c, above which feedback-induced modes may prevent stabilization of CW emission, will also remain valid for an all-optical DFC of other target states.

Acknowledgments

V.Z.Tronciu acknowledges AvH support and expresses his gratitude for the hospitality in the groups Laser Dynamicsät WIAS and Photonik at HUB

References

[1] R.F. Kazarinov and Ch.H. Henry, *The relation of line narrowing and chirp reduction resulting from the coupling of a semiconductor laser to a passive resonator*, IEEE J. Quantum Electron. **23**, No. 9, pp. 1401-1409 (1987).

[2] R.W.P. Drever et al., *Laser phase and frequency stabilization using an optical-resonator*, Appl. Phys. B **31,** No. 2, pp. 97-105 (1983).

[3] B. Dahmani, L. Hollberg, and R. Drullinger, *Frequency stabilization of semiconductor lasers by resonant optical feedback*, Optics Letters **12**, No. 11, pp. 876-878 (1987).

[4] C.E. Wieman and L. Hollberg, *Using diode lasers for atomic physics*, Rev. Sci. Instrum. **62**, No. l, pp. 1-20 (1991).

[5] V.V. Vassiliev, S.M. Il'ina, and V.L. Velichansky, *Diode laser coupled to a high-Q microcavity via a GRIN lens*, Appl. Phys. B **76**, pp. 521-523 (2003).

[6] K. Numata, A. Kemery, and J. Camp, *Thermal-noise limit in the frequency stabilization of lasers with rigid cavities*, Phys. Rev. Letters **93**, 250602 (2004).

[7] K. Pyragas, Phys.Lett. A **170**, pp. 421-428 (1992).

[8] J.E.S. Sokolar, D.W. Sukow, and D.J. Gauthier, Phys.Rev. E **50**, 3245 (1994).

[9] D.W. Sukow, M.E. Bleich, D.J. Gauthier, and J.E.S. Socolar, *Controlling chaos in a fast diode resonator using extended time-delay autosynchronization: Experimental observations and theoretical analysis*, Chaos **7**, pp. 560-576 (1997).

[10] A.G. Balanov, N.B. Janson, and E. Schöll, *Delayed feedback control of chaos: Bifurcation analysis*, Phys. Rev. E **71**, 016222 (2005).

[11] D. Goldobin, M. Rosenblum, and A. Pikovsky, *Controlling oscillator coherence by delayed feedback*, Phys. Rev. E **67**, 061119 (2003).

[12] N.B. Janson, A.G. Balanov, and E. Schöll, *Delayed feedback as a means of control of noise-induced motion*, Phys. Rev. Lett. **93**, 010601 (2004).

[13] W. Lu, R.G. Harrison, *Controlling chaos using continuous interference feedback: proposal for all optical devices*, Optics Communications **109**, pp. 457-461 (1994).

[14] C. Simmendinger and O. Hess, *Controlling delay-induced chaotic behavior of a semiconductor laser with optical feedback*, Phys. Lett. A **216**, pp. 97-105 (1996).

[15] Y. Liu and J. Ohtsubo, *Dynamics and chaos stabilization of semiconductor lasers with optical feedback from an interferrometer*, IEEE J. Quantum Electron. **33**, No. 7, pp. 1163-1169 (1997).

[16] S. Bauer et al., *Nonlinear dynamics of semiconductor lasers with active optical feedback*, Phys. Rev. E **69**, p. 016206, 2004.

[17] R. Lang and K. Kobayashi, IEEE J. Quantum Electron. QE -**16**, pp.347-355 (1980).

[18] Haegeman et al., Phys. Rev E **66**, 046216 (2002).

[19] M. Wolfrum and D. Turaev, *Instabilities of lasers with moderately delayed optical feedback*, Opt. Commun. **212**, pp. 127-138 (2002).

[20] K. Engelborghs, T. Luzyanina, and G. Samaey, DDE-BIFTOOL v. 2.00: *A Matlab package for bifurcation analysis of delay differential equations*, Technical Report TW-330, Department of Computer Science, K.U.Leuven, Leuven, Belgium, 2001.

[21] G.P. Agrawal and N.K. Dutta, *Semiconductor lasers*, 2nd edition, van Nostrand Reinhold, New-York, 1993.